

# Effect of hot isostatic pressing processing parameters on microstructure and properties of Ti60 high temperature titanium alloy

\*Tian-yu Liu<sup>1,2</sup>, Kun Shi<sup>1,2</sup>, Jun Zhao<sup>1,2</sup>, Shi-bing Liu<sup>1,2</sup>, You-wei Zhang<sup>1,2</sup>, Hong-yu Liu<sup>1,2</sup>, Tian-yi Liu<sup>1,2</sup>, Xiao-ming Chen<sup>1,2</sup>, and Xin-min Mei<sup>1,2</sup>

1. Shenyang Research Institute of Foundry Co., Ltd., Shenyang 110022, China

2. State Key Laboratory of Light Alloy Casting Technology for High-end Equipment, Shenyang 110022, China

**Abstract:** Hot isostatic pressing parameters are critical to Ti60 high temperature titanium alloy castings which have wide application perspective in aerospace. In order to obtain optimal processing parameters, the effects of hot isostatic pressing parameters on defects, composition uniformity, microstructure and mechanical properties of Ti60 cast high temperature titanium alloy were investigated in detail. Results show that increasing temperature and pressure of hot isostatic pressing can reduce defects, especially, the internal defects are substantially eliminated when the temperature exceeds 920 °C or the pressure exceeds 125 MPa. The higher temperature and pressure can improve the microstructure uniformity. Besides, the higher pressure can promote the composition uniformity. With the temperature increases from 880 °C to 960 °C,  $\alpha$ -laths are coarsened. But with increasing pressure, the grain size of prior- $\beta$  phase, the widths of  $\alpha$ -laths and  $\alpha$ -colony are reduced. The tensile strength of Ti60 alloy is 949 MPa, yield strength is 827 MPa, and the elongation is 11% when the hot isostatic pressing parameters are 960 °C/125 MPa/2 h, which exhibits the best match between the strength and plasticity.

**Keywords:** hot isostatic pressing; processing parameters; Ti60 titanium alloy; defects; composition uniformity; microstructure; mechanical properties

CLC numbers: TG146.23

Document code: A

Article ID: 1672-6421(2023)01-049-08

## 1 Introduction

High temperature titanium alloys, such as IMI-834 (Ti-6.0Al-4.0Sn-3.5Zr-0.5Mo-0.7Nb-0.35Si, wt.%), Ti-1100 (Ti-6.0Al-2.9Sn-4.2Zr-0.39Mo-0.41Si, wt.%), BT-36 (Ti-6.2Al-2.0Sn-3.6Zr-0.7Mo-5.0W-0.15Si, wt.%) and Ti60 (Ti-5.8Al-4.0Sn-3.5Zr-0.4Mo-0.4Nb-1.0Ta-0.4Si-0.06C, wt.%), etc., have been widely used in jet engines and compressor discs and blades due to their high specific strength, high specific stiffness, low density, excellent high temperature properties and corrosion resistance [1-3]. Among them, Ti60 alloy, a novel near- $\alpha$  titanium alloy developed on the basis of IMI-834, has up to 600 °C of maximum service temperature [4]. Compared with IMI-834 alloy, it is clear that Ti60 alloy contains more Si elements which can improve the creep performance at 600 °C service temperature, and a small

amount of Ta and C elements can improve its heat resistance and widen ( $\alpha+\beta$ ) phase region. At present, although Ti60 alloy has attracted extensive attention, it is difficult to form via forging and rolling because of its high chemical activity and low plasticity, limiting the application in most fields.

Owing to near-net shape, high complexity and high dimension accuracy, casting is one of the promising manufacturing technologies which can fabricate high performance large, thin-walled, complex Ti60 parts [5]. However, large number of defects such as shrinkage porosity and shrinkage cavity will be formed as the result of the characteristic of high thermal conductivity and high expansion coefficient in Ti60 alloy during the solidification process, which seriously decreases the mechanical properties and service safety of the castings [6, 7]. Hot isostatic pressing (HIP) can compact the internal defects via high temperature and high pressure, which is widely used in the post-processing of castings to improve the mechanical properties and reliability, especially the fatigue properties [8]. Xu et al. [9] investigated the effects of HIP temperature on as-cast Ti-6Al-4V, and suggested that defects decreased with

### \*Tian-yu Liu

Male, Ph. D. His research interests mainly focus on structural modeling of disordered materials, alloy design, and laser additive manufacturing.

E-mail: liutianyusrif@163.com

Received: 2022-05-19; Accepted: 2022-10-11

the increasing of HIP temperature, and even completely closed above 920 °C. The study results of Jiang et al. [10] showed that the porosity defects in additive manufacturing Ti60 alloy disappeared after HIP, and the elongation increased from 6.5% to 12.0%. In addition, being similar to annealing, the microstructure and mechanical properties depended on the HIP processing parameters. Zhang et al. [11] found that Ti-6Al-4V exhibited a better balance of properties at 930 °C of HIP temperature than those at 880 °C or 1,020 °C at the pressure 100 MPa. Chang et al. [12] studied the effect of HIP temperature on the microstructure and properties of Inconel 718 alloy, and the results showed that as the HIP holding temperature increased from 1,140 °C to 1,260 °C, the tensile strength decreased from 1,116 MPa to 976 MPa, and the elongation increased from 5% to 24%.

HIP processing parameters, especially HIP temperature and pressure play an important role in castings. However, there are few investigations about the effect of HIP parameters on the internal defects, microstructure and properties of Ti60 alloy in the open literature. Besides, it is very important that choose appropriate HIP processing parameters to achieve excellent comprehensive properties, especially the high elongation guaranteeing the service safety. Therefore, in this study, the effect of HIP processing parameters on internal defects, composition uniformity, microstructure, microhardness and tensile properties of Ti60 alloy was studied in detail, which can provide theoretical basis and technical support for casting Ti60 alloy parts.

## 2 Experimental procedure

Commercially pure Ti, Al, Ta, Zr, and master alloy Al-Mo, Al-Sn, Al-Nb, Al-Si, were used to prepare a nominal composition of Ti60 alloy. The purity of these elements was tested to be higher than 99.5%. The Ti60 alloy samples were fabricated using a vacuum induction suspension melting furnace, and the melting parameters were chosen as melting power 150–200 kW, melting

time 10–20 min. Before melting, the vacuum degree of the melting chamber should be  $5 \times 10^{-1}$  Pa, then argon was purged into the chamber to prevent the oxidation of the alloy during melting. In order to ensure composition homogeneity, Ti60 alloy was melted repeatedly at least three times. Then, the alloy rods with the size of  $\varnothing 20$  mm  $\times$  150 mm were prepared by using a graphite mold, as shown in Fig. 1. The composition of Ti60 alloys was analyzed by the ICP Inductively Coupled Plasma Emission Spectrometer, and the composition is listed in Table 1.

The samples were HIP treated using a QIH-16 HIP furnace with the heating rate of  $10 \text{ }^\circ\text{C}\cdot\text{min}^{-1}$ , the pressure increasing rate of  $1 \text{ MPa}\cdot\text{s}^{-1}$ , and gaseous environment 99.998% argon purity. Two groups of HIP processing parameters were used to investigate the effects of temperature and pressure on the microstructure and properties of Ti60 alloy, respectively, as shown in Table 2. After holding for 2 h, the samples were cooled to below 300 °C and then removed from the furnace.

After grinding, polishing, and etching (etching solution: 5% HF +12% HNO<sub>3</sub>+83% H<sub>2</sub>O, volume fraction), the microstructure was observed via ZEISS Axio Ver. Al optical microscopy (OM) and ZEISS EVO MA25 scanning electron microscopy (SEM). The width of  $\alpha$ -laths at different HIP process parameters was examined from the SEM morphology images (at least 3 images) using Image-Pro Plus 6.0 software. The elemental distributions were measured by using Oxford EDS.

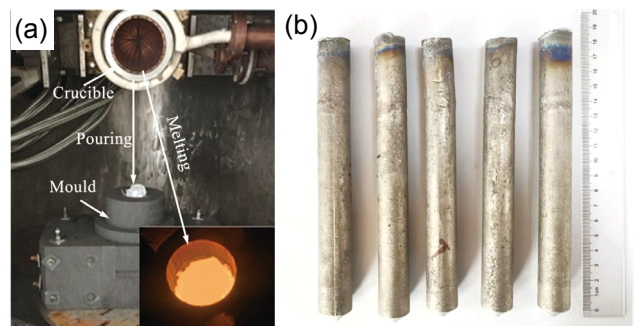


Fig. 1: Vacuum induction suspension melting and pouring (a), and Ti60 alloy rods (b)

Table 1: Composition of Ti60 titanium alloy (wt.%)

Al	Sn	Zr	Mo	Nb	Ta	Si	Ti
5.61	3.69	3.45	0.99	0.40	0.20	0.38	Bal.

Uniaxial tensile tests were carried out via CSS-1120 universal tensile testing machine with a strain rate of  $1 \times 10^{-3} \text{ s}^{-1}$  at room

Table 2: Hot isostatic pressing process

Samples	Temperature (°C)	Time (h)	Pressure (MPa)
1	880	2	125
2	920	2	125
3	960	2	125
4	920	2	105
5	920	2	145

temperature, in which the size of the test sample is shown in Fig. 2. Microhardness tests were conducted on the HVS-1000 apparatus with a load of 10 kg for 15 s, where each sample was tested for five times at least.

## 3 Results and discussion

### 3.1 Effect of HIP processing parameters on internal defects

Figure 3 shows the effect of HIP processing parameters on the internal defects of Ti60 alloy. It is clear that there are many metallurgical defects inside the Ti60 alloy in as-cast condition,

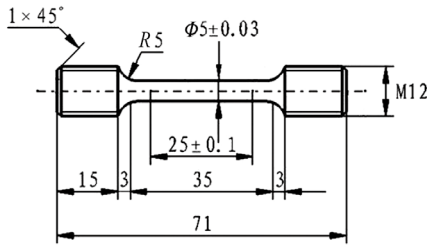


Fig. 2: Schematic diagram of tensile test specimens (unit: mm)

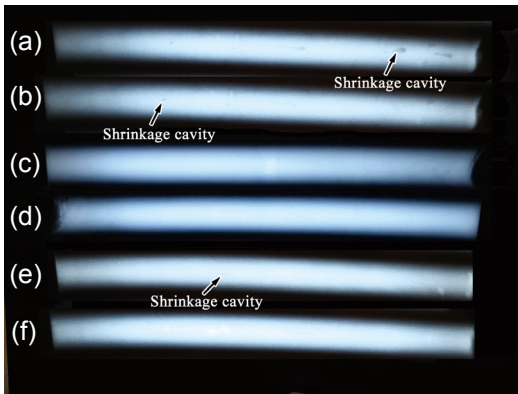


Fig. 3: Effect of HIP parameters on internal defects in Ti60 alloy rods: (a) as-cast; (b) 880 °C/125 MPa/2 h; (c) 920 °C/125 MPa/2 h; (d) 960 °C/125 MPa/2 h; (e) 920 °C/105 MPa/2 h; (f) 920 °C/145 MPa/2 h

such as shrinkage cavities. After HIP treatment, the defects are significantly reduced, especially when the HIP processing parameters are 920 °C/125 MPa/2 h, 960 °C/125 MPa/2 h, and 920 °C/145 MPa/2 h, no obvious defects are found, as shown in Figs. 3(c, d, f). The low temperature and pressure, 880 °C/125 MPa/2 h and 920 °C/105 MPa/2 h, are unfavorable for the plastic deformation and element diffusion, which makes the cavities incompletely closed, as shown in Figs. 3(b, e).

According to the shell model<sup>[13]</sup>, the minimum applied stress for plastic deformation of the metal around the cavity is:

$$\sigma_{lim} = -\frac{2\sigma_y}{3} \ln \rho \quad (1)$$

where  $\sigma_{lim}$  is the minimum applied stress,  $\sigma_y$  is the yield strength,  $\rho$  is the porosity. Therefore, when the actual applied stress  $\sigma$  satisfies:  $\sigma > \sigma_{lim}$ , plastic deformation occurs which can close the cavity. It is well-known that the yield strength will be reduced at high temperature, making the  $\sigma_{lim}$  reduced. Combining with high pressure, the relationship of  $\sigma > \sigma_{lim}$  is satisfied, so, Ti60 alloy undergoes plastic deformation in the HIP process which closes the cavity.

### 3.2 Effect of HIP pressure parameters on elemental distribution

Figures 4 and 5 present the effect of HIP pressure parameters on elemental distribution. The EDS analysis reveals that the fluctuation range of Zr, Al, Si, and Sn elements is larger than the Nb, Mo, and Ta elements at the HIP processing parameters of 920 °C/105 MPa/2 h. But, at the HIP processing parameters of 920 °C/145 MPa/2 h, which has a higher pressure, the fluctuation range of Zr, Al, Si, Sn, Nb, Mo, and Ta elements is smaller than at the processing parameters of lower pressure, suggesting that high pressure benefits to improve composition uniformity. Theoretically, according to Eq. (2)<sup>[14]</sup>:

$$D_{eff} = D_v + 5D_c \left( \frac{\frac{\sigma}{\sqrt{3}} - 0.75 \times 10^{-3} G}{\alpha G} \right)^2 \quad (2)$$

where  $D_{eff}$  is the effective diffusion coefficient,  $D_v$  is the diffusion coefficient on the lattice,  $D_c$  is the dislocation channel diffusion coefficient,  $\alpha$  is a constant, and  $G$  is the free energy. It is well-known that HIP can significantly increase

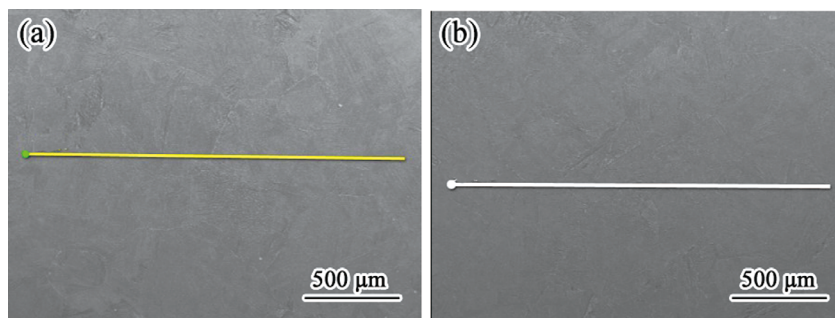


Fig. 4: SEM images of EDS: (a) 920 °C/105 MPa/2 h; (b) 920 °C/145 MPa/2 h

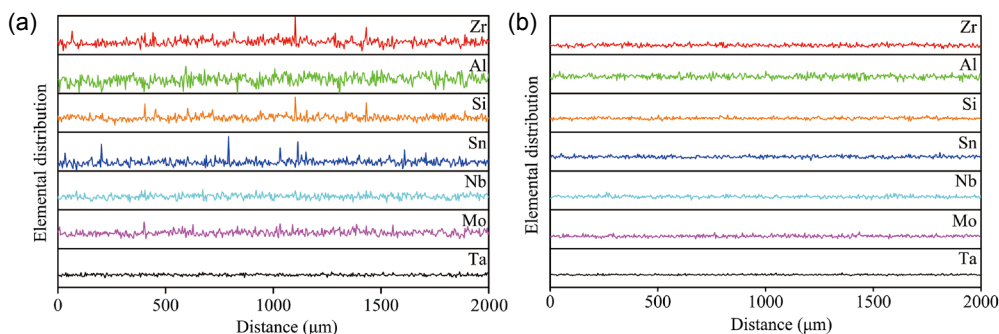


Fig. 5: Effect of HIP pressure on elemental distribution in Fig. 4: (a) 920 °C/105 MPa/2 h; (b) 920 °C/145 MPa/2 h

the dislocation because of applied stress, and the dislocation density increases with the increase of HIP pressure [14]. The increase of dislocation density is beneficial to increase  $D_c$ , and accelerate the diffusion of alloy elements leading to improved composition uniformity. Whether pressure promotes or hinders the diffusion of alloy composition is a long-debated issue. Such as, Coble et al. [15] proposed that diffusion could be promoted at high pressure. However, Nachtrieb et al. [16] believed that the stress increased the diffusion activation energy, reducing the constant factor  $D_0$  of the diffusion coefficient. Based on this experiment, it is suggested that HIP pressure can promote the alloy elements diffusion which improves composition uniformity.

### 3.3 Effect of HIP processing parameters on microstructure

The low magnification OM images at different HIP processing parameters are shown in Fig. 6. The microstructure consists of equiaxed prior- $\beta$  grains and  $\alpha$ -laths. Since HIP temperature is below  $\beta$  transus temperature ( $T_\beta \approx 970^\circ\text{C}$ ), the grain size of  $\beta$

phase does not change significantly with the increase of the HIP temperature. However, with increasing HIP pressure, the prior- $\beta$  grains size decreases slightly due to external forces. In addition, the shrinkage cavities can be observed at the HIP processing parameters of  $880^\circ\text{C}/125\text{ MPa}/2\text{ h}$  and  $920^\circ\text{C}/105\text{ MPa}/2\text{ h}$ , as shown in Figs. 6(a, d).

Figure 7 exhibits high magnification OM images at different HIP processing parameters. It shows that the microstructure within the prior- $\beta$  grains contains grain boundary  $\alpha$  phase ( $\alpha_{\text{GB}}$ ) and Widmanstatten  $\alpha$ -laths. Obviously, the Widmanstatten consists of  $\alpha$ -laths with uneven thickness at the HIP processing parameters of  $880^\circ\text{C}/125\text{ MPa}/2\text{ h}$  and  $920^\circ\text{C}/105\text{ MPa}/2\text{ h}$ , as shown in Figs. 7(a, d), suggesting the low microstructure homogeneity. But with increasing HIP temperature or pressure, as shown in Figs. 7(b, c, e), it is clear that the microstructure is composed of  $\alpha$ -laths with similar size, especially at the HIP processing parameters of  $920^\circ\text{C}/145\text{ MPa}/2\text{ h}$ , which indicates that the microstructure homogeneity is improved. It is evident that high pressure is more conducive to improve the microstructure homogeneity than high temperature.

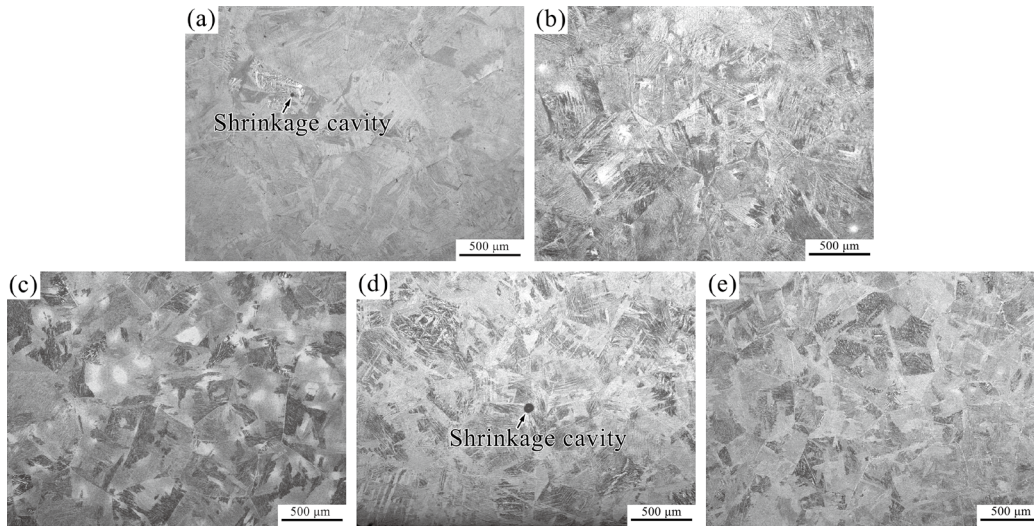


Fig. 6: Low magnification OM images under different HIP parameters: (a)  $880^\circ\text{C}/125\text{ MPa}/2\text{ h}$ ; (b)  $920^\circ\text{C}/125\text{ MPa}/2\text{ h}$ ; (c)  $960^\circ\text{C}/125\text{ MPa}/2\text{ h}$ ; (d)  $920^\circ\text{C}/105\text{ MPa}/2\text{ h}$ ; (e)  $920^\circ\text{C}/145\text{ MPa}/2\text{ h}$

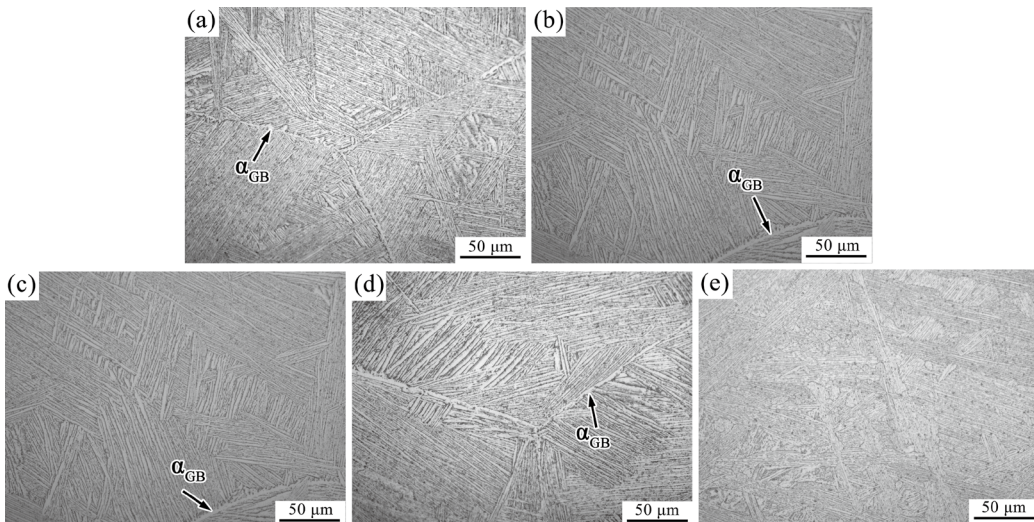


Fig. 7: High magnification OM images at different HIP parameters: (a)  $880^\circ\text{C}/125\text{ MPa}/2\text{ h}$ ; (b)  $920^\circ\text{C}/125\text{ MPa}/2\text{ h}$ ; (c)  $960^\circ\text{C}/125\text{ MPa}/2\text{ h}$ ; (d)  $920^\circ\text{C}/105\text{ MPa}/2\text{ h}$ ; (e)  $920^\circ\text{C}/145\text{ MPa}/2\text{ h}$

Figure 8 gives SEM images at different HIP processing parameters, and Fig. 9 displays the changes in the width of  $\alpha$ -laths at different HIP processing parameters. The width of  $\alpha$ -laths is increased with increasing HIP temperature, but increasing pressure reduces the width of  $\alpha$ -laths. It clearly shows that the width of  $\alpha$ -laths increases from 1.09  $\mu\text{m}$  to 1.61  $\mu\text{m}$  with increasing HIP temperature from 880  $^{\circ}\text{C}$  to 960  $^{\circ}\text{C}$  in

which HIP pressure and time are constant (125 MPa/2 h), as shown in Fig. 9(a). Conversely, the width of  $\alpha$ -laths decreases from 1.46  $\mu\text{m}$  to 0.95  $\mu\text{m}$  with increasing HIP pressure from 105 MPa to 145 MPa in which HIP temperature and time are constant (920  $^{\circ}\text{C}/2\text{ h}$ ), as shown in Fig. 9(b). Furthermore, it should be point out that the width of  $\alpha$ -laths does not show dramatical variation with increasing HIP pressure from 105 MPa to 125 MPa.

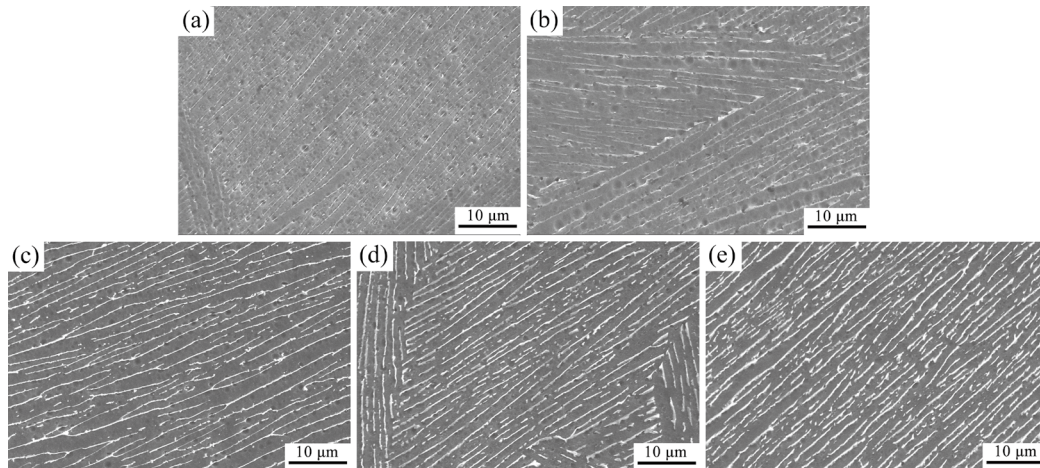


Fig. 8: SEM images at different HIP parameters: (a) 880  $^{\circ}\text{C}/125\text{ MPa}/2\text{ h}$ ; (b) 920  $^{\circ}\text{C}/125\text{ MPa}/2\text{ h}$ ; (c) 960  $^{\circ}\text{C}/125\text{ MPa}/2\text{ h}$ ; (d) 920  $^{\circ}\text{C}/105\text{ MPa}/2\text{ h}$ ; (e) 920  $^{\circ}\text{C}/145\text{ MPa}/2\text{ h}$

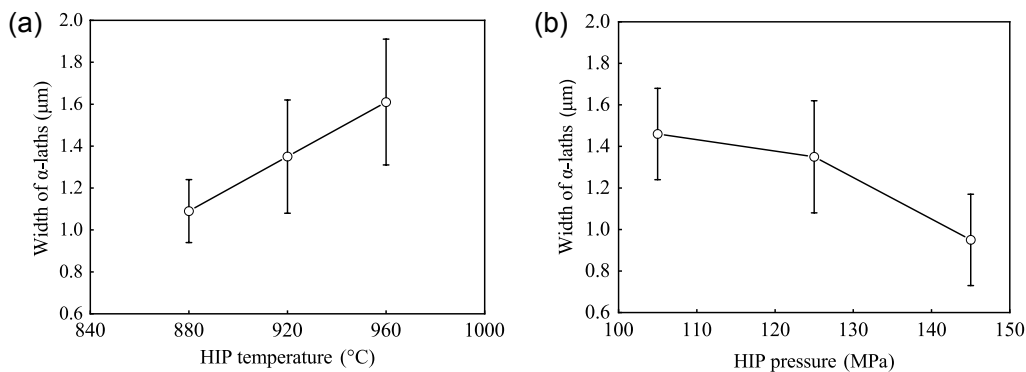


Fig. 9: Changes in width of  $\alpha$ -laths at different HIP parameters: (a) width of  $\alpha$ -laths as a function of HIP temperature; (b) width of  $\alpha$ -laths as a function of pressure

### 3.4 Effect of HIP processing parameters on mechanical properties

The microhardness at different HIP processing parameters is shown in Fig. 10. With increasing HIP temperature from 880  $^{\circ}\text{C}$  to 960  $^{\circ}\text{C}$  in which HIP pressure and time are constant (125 MPa/2 h), the microhardness decreases from 333 HV to 320 HV, as shown in Fig. 10(a). In addition, with increasing HIP pressure from 105 MPa to 125 MPa in which HIP temperature and time are constant (920  $^{\circ}\text{C}/2\text{ h}$ ), the microhardness is similar, about 326 HV, but increases to 334 HV with increasing HIP pressure to 145 MPa. Apparently, the smaller pressure does not have an effect on the microhardness, due to the slight change of grain size of  $\alpha$  and  $\beta$  phases.

The result of the room temperature tensile testing at different HIP processing parameters is presented in Fig. 11. With increasing HIP temperature from 880  $^{\circ}\text{C}$  to 960  $^{\circ}\text{C}$  in which HIP pressure and time are constant, it can be seen that the

tensile strength of Ti60 alloy at room temperature decreases from 970 MPa to 957 MPa, the yield strength decreases from 857 MPa to 827 MPa, and the elongation increases from 4% to 11%, respectively. As the grain size of  $\alpha$  phase increases from 1.09  $\mu\text{m}$  to 1.61  $\mu\text{m}$ , the slip length of dislocation increases which reduces dislocation plugging, thereby reducing the strength and increasing the elongation. But the mechanical properties of Ti60 alloy change nonlinearly as HIP pressure increases from 105 MPa to 145 MPa in which HIP temperature and time are constant. At the HIP processing parameters of 920  $^{\circ}\text{C}/105\text{ MPa}/2\text{ h}$ , 920  $^{\circ}\text{C}/125\text{ MPa}/2\text{ h}$  and 920  $^{\circ}\text{C}/145\text{ MPa}/2\text{ h}$ , the tensile strength of Ti60 alloy is 967 MPa, 959 MPa and 982 MPa, the yield strength is 859 MPa, 842 MPa, and 861 MPa, and the elongation is 3%, 6%, and 5%, respectively. It can be seen that the strength is similar at the HIP processing parameters of 920  $^{\circ}\text{C}/105\text{ MPa}/2\text{ h}$  and 920  $^{\circ}\text{C}/125\text{ MPa}/2\text{ h}$ , while the strength improved at the HIP processing parameters of 920  $^{\circ}\text{C}/145\text{ MPa}/2\text{ h}$ .

According to the Hall-Petch relation<sup>[17]</sup>:

$$\sigma_y = \sigma_0 + kd^{-1/2} \quad (3)$$

where  $\sigma_y$  is yield strength,  $\sigma_0$  and  $k$  are material constants, and  $d$  is the average grain diameter. The Hall-Petch relation suggests that the yield strength increases as the prior- $\beta$  grains size decreases. Besides, decreasing  $\alpha$ -laths from 1.46  $\mu\text{m}$  to 0.95  $\mu\text{m}$  [Fig. 9(b)] benefits to improve dislocation density, which enhance the strength. At the HIP processing parameters of 920 °C/105 MPa/2 h, internal defects lead to reduced elongation.

Figure 12 shows work-hardening rate curves of the Ti60 alloy at different HIP parameters. As shown in Fig. 11(a) there are three distinct stages in the curves for the deformed Ti60, labeled as A, B, and C, respectively. In Stage A, the work hardening rate curves sharply decreases for the HIP processing parameters of 880 °C/125 MPa/2 h, 920 °C/125 MPa/2 h, 920 °C/105 MPa/2 h, and 920 °C/145 MPa/2 h, as shown in Fig. 12(a), mainly due to alloys undergo elastoplastic transition<sup>[18-20]</sup>. Besides, in

Stage A, all curves are nearly parallel to each other, suggesting that the evolutionary rate of dislocation density is at the same level during the initial beginning of plastic deformation<sup>[21]</sup>. In Stage B, the work hardening rate stays at a constant level for the HIP processing parameters of 880 °C/125 MPa/2 h and 920 °C/145 MPa/2 h, but notably increase of strain for the HIP processing parameters of 920 °C/125 MPa/2 h and 920 °C/105 MPa/2 h. In Stage C, the work hardening rate further decreases for the HIP processing parameters of 880 °C/125 MPa/2 h, 920 °C/125 MPa/2 h, 920 °C/105 MPa/2 h, and 920 °C/145 MPa/2 h, but decreases slowly than those of Stage A.

For the HIP processing parameters of 960 °C/125 MPa/2 h, as shown in Fig. 12(b), the work hardening capacity shows a small difference with other curves in Stage A, but still displays a beneficial effect on suppressing rapid decline of work hardening rate. In Stage B, the work hardening rate curve shows a great difference compared to those at other HIP processing parameters. The slope of work hardening slowly

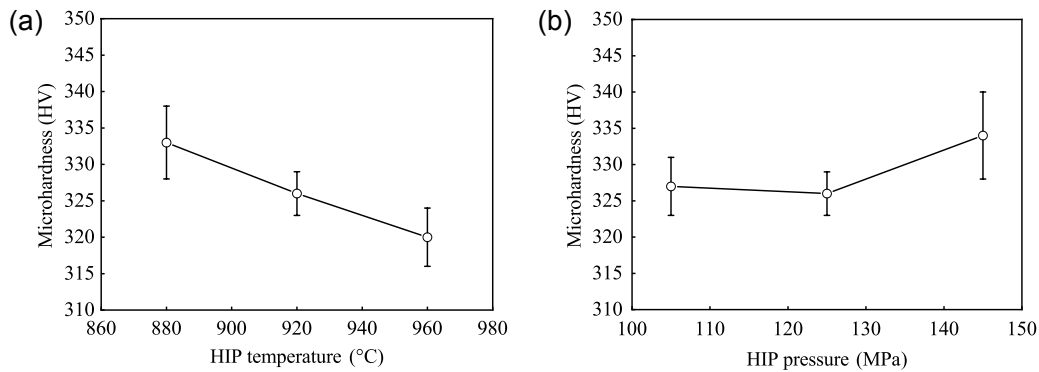


Fig. 10: Effect of HIP parameters on Vickers hardness: (a) HIP temperature; (b) HIP pressure

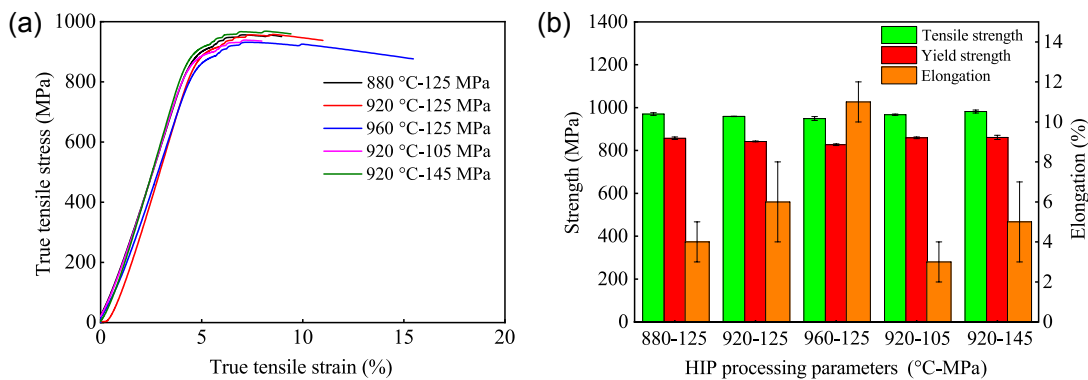


Fig. 11: Room temperature tensile properties of Ti60 alloy at different HIP parameters

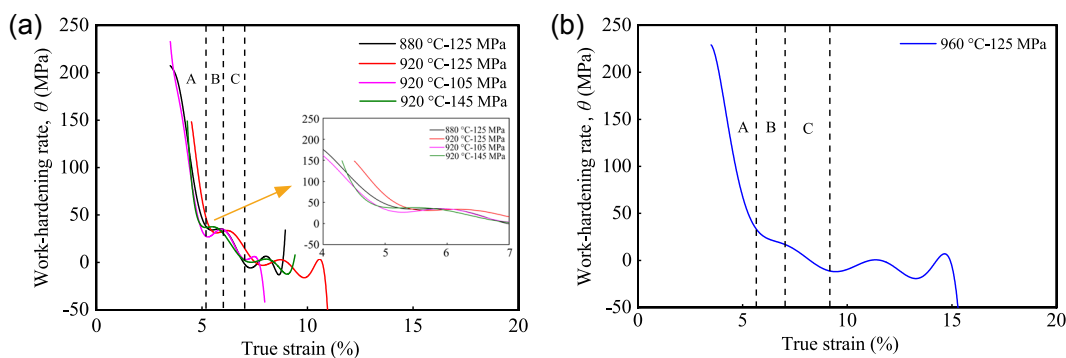


Fig. 12: Curves of work hardening rate of Ti60 alloy at different HIP parameters

decreases, indicating that the dislocation packing is relatively slow. Besides, in Stage C, the slope of the work hardening rate curves slowly decreases relative to other samples, which is beneficial to improve the ductility of the alloy. In general, a homogeneous microstructure is conducive to enhance the uniform deformation ability during deformation, and a coarsen microstructure is beneficial to weaken the dislocation packing. For the HIP processing parameters of 960 °C/125 MPa/2 h, the alloy shows a relatively homogeneous and coarsen microstructure (in Fig. 7), and thus gives rise to a better work hardening capacity and uniform deformation ability. In all, those indicate a better plasticity for this HIP processing parameter.

The work hardening ability of alloys also can be predicted

by the strain hardening exponent  $n$ <sup>[22, 23]</sup>. The larger value of  $n$  indicates greater work hardening.

$$\sigma = k\varepsilon^n \quad (4)$$

where  $n$  is the strain hardening exponent which suggests the work hardening ability,  $k$  is the strength coefficient,  $\sigma$  is the true stress, and  $\varepsilon$  is the true strain. In order to obtain the value of  $n$ , the  $\lg\sigma = n\lg\varepsilon + \ln k$  curves are given, as shown in Fig. 13(a). Further, the work hardening exponent ( $n$ ) values are shown in Fig. 13(b). It is clear that the value of  $n$  is the maximum with the HIP processing parameters of 960 °C/125 MPa/2 h. A high work hardening ability can effectively distribute plastic deformation and delay the onset of necking, which result in a larger elongation.

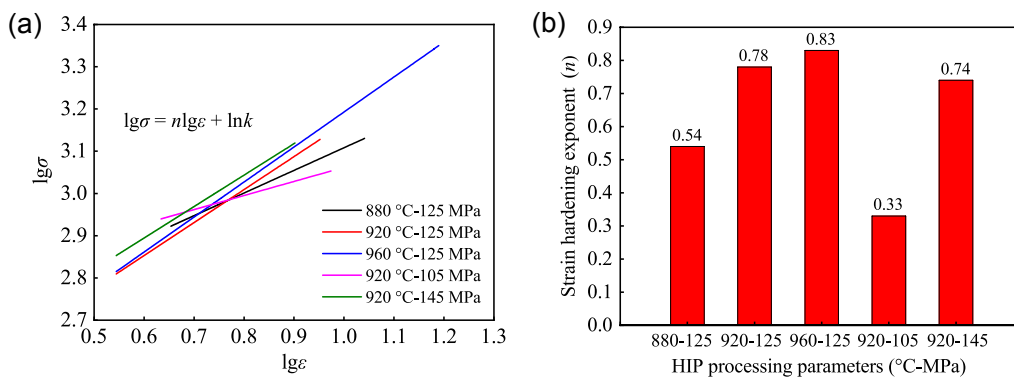


Fig. 13:  $\lg\sigma$ - $\lg\varepsilon$  curves by the true stress and true strain (a), and work hardening exponent ( $n$ ) value (b)

### 3.5 Effect of HIP processing parameters on fracture morphology

Figure 14 gives fracture morphologies of room temperature tensile samples at different HIP parameters. It is obvious that the fracture morphologies essentially exhibit cleavage facets at the HIP processing parameters of 880 °C/125 MPa/2 h, 920 °C/125 MPa/2 h, 920 °C/105 MPa/2 h, and 920 °C/145 MPa/2 h, as shown in Figs. 14(a, b, d, e). So, the fracture mechanism can be considered as cleavage fracture mode. It is well-known that  $\alpha$  phase with hexagonal close-packed (HCP) structure has lower plasticity than the  $\beta$  phase with body-centered cubic (BCC)

structure, which causes cracks to propagate along  $\alpha$ -lath quickly and it is easy to form the smooth cleavage facets. The  $\beta$  phase, owing to its good plasticity, experiences drastic plastic deformation before rupture, and then the white tearing ridge is formed adjacent to the primary  $\alpha$  phase. Therefore, the fracture mechanism can be identified as a mixed fracture mode at the HIP processing parameter of 960 °C/125 MPa/2 h, but the ductile fracture is the dominate due to exist of many dimples, as shown in Fig. 13(c). The dimples characteristics of the fracture morphology support the higher value of elongation.

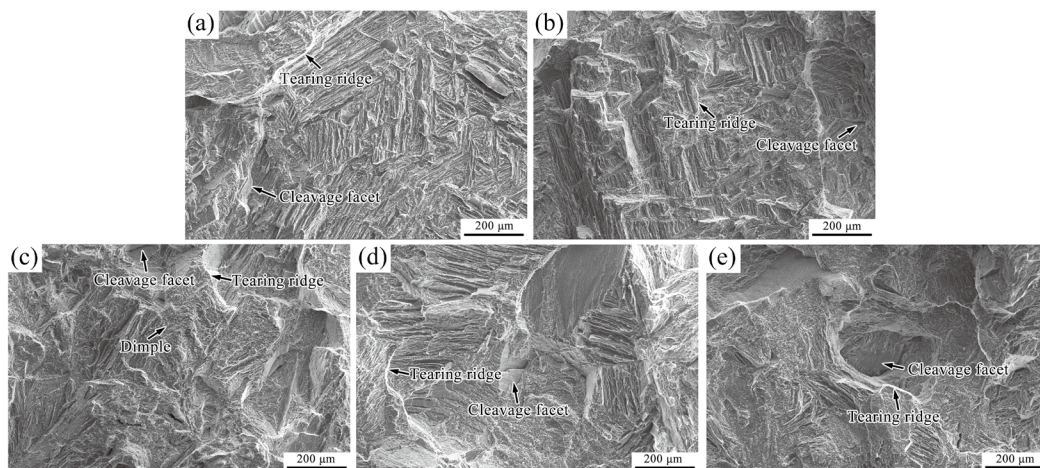


Fig. 14 : Fracture morphologies of room temperature tensile at different HIP parameters: (a) 880 °C/125 MPa/2 h; (b) 920 °C/125 MPa/2 h; (c) 960 °C/125 MPa/2 h; (d) 920 °C/105 MPa/2 h; (e) 920 °C/145 MPa/2 h

## 4 Conclusions

In this study, the effects of HIP processing parameters, including temperature and pressure, on porosity, composition uniformity, microstructure and mechanical properties of Ti60 alloy were studied. The following conclusions can be obtained:

(1) Increasing HIP temperature and pressure both reduce the number of metallurgical defects, and no obvious defects are found at processing parameters of 920 °C/125 MPa/2 h, 960 °C/125 MPa/2 h and 920 °C/145 MPa/2 h.

(2) Increasing HIP temperature and pressure are beneficial to improve the composition and microstructure uniformity.

(3) After HIP with the processing parameters of 960 °C/125 MPa/2 h, the tensile strength of Ti60 alloy is 949 MPa, the yield strength is 827 MPa, the elongation is 11%, which exhibits the best match between the strength and plasticity.

## Acknowledgement

This work was financially supported by the National Key Research and Development Program of China (Grant No. 2020YFB2008300).

## Conflict of interest

The authors declare that they have no conflict of interest.

## References

- [1] Wanjara P, Jahazi M, Monajati H, et al. Influence of thermomechanical processing on microstructural evolution in near- $\alpha$  alloy IMI834. *Materials Science and Engineering: A*, 2006, 416(1-2): 300–311.
- [2] Lee D H, Nam S W, Choe S J. Effect of  $\alpha$  lamellae width on creep-fatigue behavior in Near- $\alpha$  Ti-1100 with lamellar structure. *Scripta Materialia*, 1999, 40(3): 265–270.
- [3] Niu Y, Hou H L, Li M Q, et al. High temperature deformation behavior of a near alpha Ti600 titanium alloy. *Materials Science and Engineering: A*, 2008, 492(1-2): 24–28.
- [4] Jia W J, Zeng W D, Zhou Y G, et al. High-temperature deformation behavior of Ti60 titanium alloy. *Materials Science and Engineering: A*, 2011, 528: 4068–4074.
- [5] Uwanyuze R S, Kanyo J E, Myrick S F, et al. A review on alpha case formation and modeling of mass transfer during investment casting of titanium alloys. *Journal of Alloys and Compounds*, 2021, 865: 158558.
- [6] Liu T Y, Liu H Y, Yao Q, et al. Microstructure and mechanical properties of laser additive manufactured novel titanium alloy after heat treatment. *China Foundry*, 2021, 18(6): 574–580.
- [7] Cen M J, Liu Y, Chen X. Inclusions in melting process of titanium and titanium alloys. *China Foundry*, 2019, 18(4): 223–231.
- [8] Lee S C, Chang S H, Tang T P, et al. Improvement in the microstructure and tensile properties of Inconel 718 superalloy by HIP treatment. *Materials Transactions*, 2006, 47(11): 2877–2881.
- [9] Xu Q, Zhou J X, Nan H, et al. Effects of hot isostatic pressing temperature on casting shrinkage densification and microstructure of Ti6Al4V alloy. *China Foundry*, 2017, 14(5): 429–434.
- [10] Jiang S, Li H X, Shi Z Q, et al. Effects of hot isostatic pressing on microstructure and tensile properties of direct laser deposited Ti60 alloy. *Infrared and Laser Engineering*, 2015, 44(1): 107–111. (In Chinese)
- [11] Zhang K, Mei J, Wain N, et al. Effect of hot-isostatic-pressing parameters on the microstructure and properties of powder Ti-6Al-4V hot-isostatically-pressed sample. *Metallurgical and Materials Transactions A*, 2010, 41(4): 1033–1045.
- [12] Chang L T, Sun W R, Cui Y Y, et al. Influences of hot-isostatic-pressing temperature on microstructure, tensile properties and tensile fracture mode of Inconel 718 powder compact. *Materials Science and Engineering: A*, 2014, 599: 186–195.
- [13] Shao C, Yin F J, Zhu X P, et al. Effect of hot isostatic pressing on densification and microstructure evolution mechanism of castings. *Powder Metallurgy Industry*, 2016, 26(2): 63–67. (In Chinese)
- [14] Zhang S Y, Sui Y J. Hip densification mechanisms for cast superalloys. *Central Iron and Steel Research Institute Technical Bulletin*, 1985, 5(S1): 77–83. (In Chinese)
- [15] Coble R L. A model for boundary diffusion controlled creep in polycrystalline materials. *Journal of Applied Physics*, 1963, 34(6): 1679–1682.
- [16] Nachtrieb N H, Resing H A, Rice S A. Effect of pressure on self-diffusion in lead. *Journal of Chemical Physics*, 1959, 31(1): 135–138.
- [17] Ren Y M, Lin X, Fu X, et al. Microstructure and deformation behavior of Ti-6Al-4V alloy by high-power laser solid forming. *Acta Materialia*, 2017, 132: 82–95.
- [18] Zhu Z H, Nie K B, Munroe P, et al. Synergistic effects of hybrid (SiC+TiC) nanoparticles and dynamic precipitates in the design of a high-strength magnesium matrix nanocomposite. *Materials Chemistry and Physics*, 2021, 259: 124048.
- [19] Han D, He J X, Guan X J, et al. Impact of short-range clustering on the multistage work-hardening behavior in Cu-Ni alloys. *Metals*, 2019, 9(2): 151.
- [20] Han D, Guan X J, Yan Y, et al. Anomalous recovery of work hardening rate in Cu-Mn alloys with high stacking fault energies under uniaxial compression. *Materials Science and Engineering: A*, 2019, 743: 745–754.
- [21] Nie K B, Zhu Z H, Munroe P, et al. Effect of extrusion speed on mixed grain microstructure and tensile properties of a Mg-2.9Zn-1.1Ca-0.5Mn nanocomposite reinforced by a low mass fraction of TiC<sub>p</sub>. *Materials Science and Engineering: A*, 2020, 796: 140223.
- [22] Li C J, Sun H F, Li X W, et al. Microstructure, texture and mechanical properties of Mg-3.0Zn-0.2Ca alloys fabricated by extrusion at various temperature. *Journal of Alloys and Compound*, 2015, 652: 122–131.
- [23] Zhu Z H, Nie K B, Munroe P, et al. Synergistic effects of hybrid (SiC+TiC) nanoparticles and dynamic precipitates in the design of a high-strength magnesium matrix nanocomposite. *Materials Chemistry and Physics*, 2021, 259: 124048.